Chapter 4

Homogenization of linear composites

[1] Mean-field homogenization schemes are an efficient way to predict the behavior of heterogeneous materials. Based on assumptions of the interaction laws between the different phases, they enable to get a prediction of the macroscopic response as well as some information on the per-phase state of deformation and stress. In comparison with the FE method, this approach is infinitely much faster. Various mean-field homogenization schemes are presented in this section and their application to linear (visco)elastic composites is examined. Furthermore, some theoretical bounds of the real response can be developed which enable to check some approximations made by the predictive methods. At first, constitutive models of the homogeneous materials are presented.

4.1 Constitutive equations

4.1.1 Linear thermo-elasticity

Consider a homogeneous linear thermo-elastic material of elastic stiffness $\boldsymbol{C}$ and thermal expansion $\boldsymbol{\alpha}$. At each point $\boldsymbol{x}$ of the material, for a given total strain $\boldsymbol{\varepsilon}$ and a change in temperature ΔT, the stress is given by:

$$\begin{aligned} \boldsymbol{\sigma}(\boldsymbol{x}) &= \boldsymbol{C} : (\boldsymbol{\varepsilon}(\boldsymbol{x}) - \boldsymbol{\varepsilon}^{th}(\boldsymbol{x})), \qquad \boldsymbol{\varepsilon}^{th}(\boldsymbol{x}) = \boldsymbol{\alpha}\Delta T(\boldsymbol{x}) && (4.1) \\ &= \boldsymbol{C} : \boldsymbol{\varepsilon}(\boldsymbol{x}) + \boldsymbol{\beta}\Delta T(\boldsymbol{x}), \qquad \boldsymbol{\beta} = -\boldsymbol{C} : \boldsymbol{\alpha}, && (4.2) \end{aligned}$$

[1] Some developments of this chapter led to the publication "Mean-field homogenization of multi-phase thermo-elastic composites: a general framework and its validation", Pierard O., Friebel C. and Doghri I., *Composites, Science and Technology*, 64 (2004), pp. 1587-1603 [80].

or equivalently,

$$\boldsymbol{\varepsilon}(\boldsymbol{x}) = \boldsymbol{C}^{-1} : \boldsymbol{\sigma}(\boldsymbol{x}) + \boldsymbol{\varepsilon}^{th}(\boldsymbol{x}), \tag{4.3}$$

where $\boldsymbol{\varepsilon}^{th}$ is the thermal strain tensor and the double dot (:) designates a tensor product contracted over two indices. The total strain $\boldsymbol{\varepsilon}$ is the sum of the mechanical and thermal strains. The latter is thus a stress free eigenstrain since a variation in temperature does not induce a stress variation. For a general material with no particular symmetry and since the conservation laws must be satisfied, the fourth-order stiffness tensor and the second-order tensor of thermal expansion have only 21 and 6 degrees of freedom, respectively.

For some materials, physical symmetries can be taken into account. A widely encountered material symmetry is transverse isotropy (the material has an axis of isotropy around which any rotation is indistinguishable). In this case, respectively 5 and 2 scalars are necessary to define the stiffness and thermal expansion tensors.

In the particular case of isotropic materials (no preferential direction), stiffness and thermal expansion tensors are depending of only two and one scalars, respectively. Equations (4.1-4.3) are then simplified to:

$$\begin{aligned} \boldsymbol{\sigma}(\boldsymbol{x}) &= \lambda[\mathrm{tr}(\boldsymbol{\varepsilon}(\boldsymbol{x}) - \boldsymbol{\varepsilon}^{th}(\boldsymbol{x}))]\mathbf{1} + 2\mu(\boldsymbol{\varepsilon}(\boldsymbol{x}) - \boldsymbol{\varepsilon}^{th}(\boldsymbol{x})), \\ \text{where } \boldsymbol{\varepsilon}^{th}(\boldsymbol{x}) &= \alpha\Delta T(\boldsymbol{x})\mathbf{1}, \end{aligned} \tag{4.4}$$

or equivalently,

$$\boldsymbol{\varepsilon}(\boldsymbol{x}) = \frac{1+\nu}{E}\boldsymbol{\sigma}(\boldsymbol{x}) - \frac{\nu}{E}[\mathrm{tr}(\boldsymbol{\sigma}(\boldsymbol{x}))]\mathbf{1} + \boldsymbol{\varepsilon}^{th}(\boldsymbol{x}), \tag{4.5}$$

where $\mathbf{1}$ is the second-order unit tensor, tr is the trace of a tensor, λ and μ are the Lamé coefficients and α is the coefficient of thermal expansion (CTE). Of course, these are related to the other coefficients classically used in isotropic linear elasticity, i.e. the Young's modulus E, the Poisson's ratio ν, the bulk modulus κ and the shear modulus $G = \mu$.

4.1.2 Linear viscoelasticity

Linear viscoelasticity is another class of linear behavior. A main difference with linear thermo-elasticity is the presence in the response of the material of an explicit time dependence due to a fading memory effect so that it is the sum of an instantaneous initial response and a time-dependent integral. If the initial state is defined at $t = 0$, the constitutive model of linear viscoelasticity reads at each point $\boldsymbol{x}$ of the homogeneous material:

$$\begin{aligned} \boldsymbol{\sigma}(\boldsymbol{x}, t) &= \boldsymbol{G}(t) : \boldsymbol{\varepsilon}(\boldsymbol{x}, 0) + \int_0^t \boldsymbol{G}(t-\tau) : \dot{\boldsymbol{\varepsilon}}(\boldsymbol{x}, \tau) d\tau \\ &= \boldsymbol{G}(t) : \boldsymbol{\varepsilon}(\boldsymbol{x}, 0) + \dot{\boldsymbol{\varepsilon}}(\boldsymbol{x}) \otimes \boldsymbol{G}, \\ \text{where } \boldsymbol{\varepsilon}(\boldsymbol{x}, 0) &= \lim_{t \to 0^+} \boldsymbol{\varepsilon}(\boldsymbol{x}, t) \end{aligned} \tag{4.6}$$

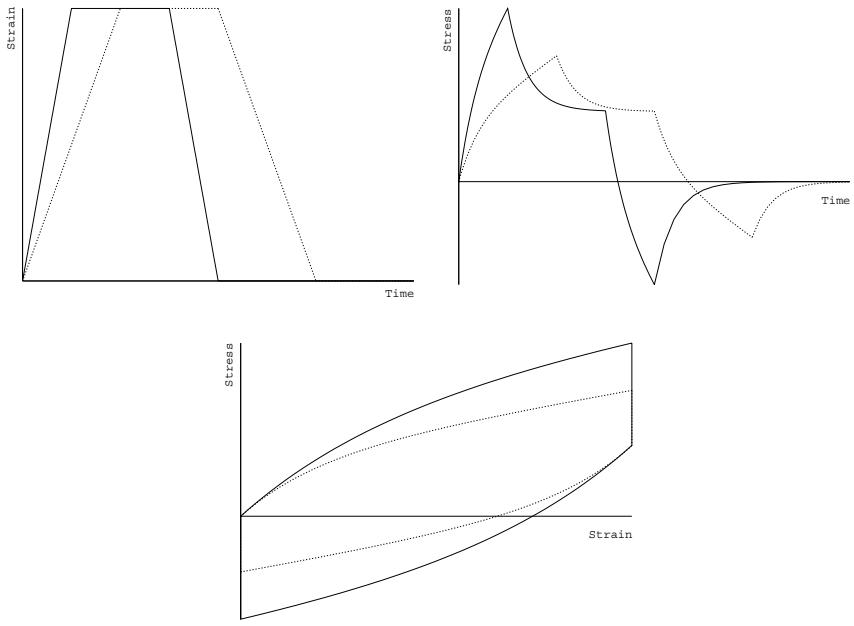

Figure 4.1: Response to a given strain loading path for a linear viscoelastic material.

or equivalently,

$$\begin{aligned} \boldsymbol{\varepsilon}(\boldsymbol{x},t) &= \boldsymbol{J}(t):\boldsymbol{\sigma}(\boldsymbol{x},0)+\int_0^t \boldsymbol{J}(t-\tau):\dot{\boldsymbol{\sigma}}(\boldsymbol{x},\tau)d\tau \\ &= \boldsymbol{J}(t):\boldsymbol{\sigma}(\boldsymbol{x},0)+\dot{\boldsymbol{\sigma}}(\boldsymbol{x})\otimes\boldsymbol{J}, \qquad (4.7) \\ \text{where } \boldsymbol{\sigma}(\boldsymbol{x},0) &= \lim_{t\to 0^+}\boldsymbol{\sigma}(\boldsymbol{x},t) \end{aligned}$$

where $\boldsymbol{G}$ is the fourth order relaxation tensor, $\boldsymbol{J}$ the fourth-order creep tensor and $\otimes$ is the classical convolution product which for two scalar functions f and g is defined by:

$$f\otimes g=\int_0^t f(\tau)g(t-\tau)d\tau. \qquad (4.8)$$

Once again, simplified expressions of the relaxation and creep tensors exist for isotropic materials (Friebel *et al.* [33]). One-dimensional linear viscoelastic constitutive law and influence of the strain rate are illustrated on figure 4.1 for two different loading paths.

The correspondence principle is a classical way to solve expressions of the form (4.6/4.7) by making use of the Laplace-Carson transform (see appendix

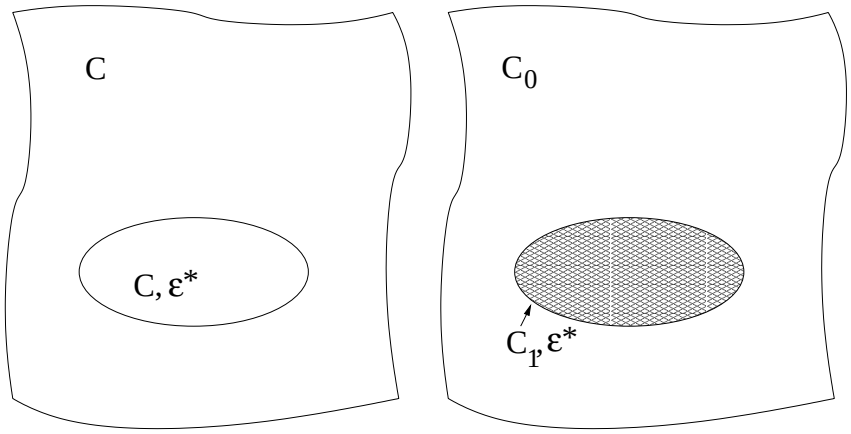

(a) Eshelby's problem. (b) Single inclusion problem.

Figure 4.2: Illustration of the results of Eshelby and Hill.

B.1). This enables to eliminate the dependence with respect to $\boldsymbol{\varepsilon}(0)$ and to rewrite these expressions under a linear elastic formalism:

$$\begin{aligned} \boldsymbol{\sigma}^*(s) &= \boldsymbol{G}^*(s) : \boldsymbol{\varepsilon}^*(s), \\ \boldsymbol{\varepsilon}^*(s) &= \boldsymbol{J}^*(s) : \boldsymbol{\sigma}^*(s), \end{aligned} \tag{4.9}$$

where f^* is the Laplace-Carson transform of the function f and s is the Laplace variable. If not singular, tensors $\boldsymbol{G}^*$ and $\boldsymbol{J}^*$ are inverse of each other.

4.2 Homogenization of isothermal elastic composites

In order to take into account some important geometrical properties (e.g.: shape and orientation of inclusions), several useful homogenization schemes are based on the solution of the Eshelby problem. From this result, the symmetric Hill's tensor is introduced which enables to guarantee some important properties of other tensors. Localization tensors are presented afterwards, from which various homogenization schemes are defined.

4.2.1 Results of Eshelby and Hill

Let us consider a homogeneous linear elastic material of stiffness $\boldsymbol{C}$ in which an embedded ellipsoidal inclusion made of the same material undergoes an eigenstrain $\boldsymbol{\varepsilon}^*$ (figure 4.2a). Eshelby [30] proved that the resulting strain field

inside the inclusion ($\boldsymbol{\varepsilon}_1$) is uniform and related to the eigenstrain through the fourth-order *Eshelby's tensor* $\mathcal{E}$:

$$\boldsymbol{\varepsilon}_1 = \mathcal{E} : \boldsymbol{\varepsilon}^*. \tag{4.10}$$

In general, $\mathcal{E}$ possesses the minor but not the major symmetries ($\mathcal{E}_{ijkl} = \mathcal{E}_{jikl} = \mathcal{E}_{ijlk}; \mathcal{E}_{ijkl} \neq \mathcal{E}_{klij}$). Analytical formulae of the Eshelby's tensor were introduced by Eshelby [30] for isotropic materials and spheroids (expressions can be found in appendix A.1). Later, Withers [108] extended this result to transversely isotropic medium, with the restriction that the direction of anisotropy is aligned with the revolution direction of the spheroid (see appendix A.2). In all other cases, a numerical evaluation of the tensor is necessary and was implemented by Gavazzi and Lagoudas [34].

The homogeneous stress field $\boldsymbol{\sigma}_1$ inside the inclusion is given by:

$$\boldsymbol{\sigma}_1 = \boldsymbol{C} : \boldsymbol{\varepsilon}_1 + \boldsymbol{\tau}, \qquad \boldsymbol{\tau} = -\boldsymbol{C} : \boldsymbol{\varepsilon}^*. \tag{4.11}$$

The second-order tensor $\boldsymbol{\tau}$ is called the *polarization tensor* and is symmetric by construction. Introducing this new tensor into (4.10) gives:

$$\boldsymbol{\varepsilon}_1 = -\boldsymbol{P} : \boldsymbol{\tau}, \qquad \boldsymbol{P} = \mathcal{E} : \boldsymbol{C}^{-1}. \tag{4.12}$$

The fourth-order tensor $\boldsymbol{P}$ is called *Hill's tensor* and relates the eigenstress due to $\boldsymbol{\varepsilon}^*$ to the strain in the inclusions.

Let's now consider a single inclusion of stiffness $\boldsymbol{C}_1$ undergoing an eigenstrain embedded in a matrix with a different stiffness ($\boldsymbol{C}_0 = \boldsymbol{C}_1 - \Delta\boldsymbol{C}$), see figure 4.2b. Stress and strain are still related through the classical relations:

$$\begin{aligned} \boldsymbol{\sigma}_0 &= \boldsymbol{C}_0 : \boldsymbol{\varepsilon}_0 \text{ in the matrix,} \\ \boldsymbol{\sigma}_1 &= \boldsymbol{C}_1 : \boldsymbol{\varepsilon}_1 + \boldsymbol{\tau}_1 \text{ in the inclusion.} \\ &= \boldsymbol{C}_0 : \boldsymbol{\varepsilon}_1 + \boldsymbol{\tau}_0, \end{aligned} \tag{4.13}$$

where $\boldsymbol{\tau}_0 = \Delta\boldsymbol{C} : \boldsymbol{\varepsilon}_1 + \boldsymbol{\tau}_1$. Following the hypothesis of Hill that $\boldsymbol{\varepsilon}_1$ is uniform in the inclusions, this relation is form similar to the homogeneous Eshelby's one so that the solution of this inhomogeneous problem is given by:

$$\boldsymbol{\varepsilon}_1 = -\boldsymbol{P}(\boldsymbol{C}_0) : \boldsymbol{\tau}_0 \Rightarrow -\boldsymbol{\tau}_1 = (\boldsymbol{C}^* + \boldsymbol{C}_1) : \boldsymbol{\varepsilon}_1; \;\; \boldsymbol{C}^* = \boldsymbol{P}^{-1} - \boldsymbol{C}_0. \tag{4.14}$$

This new fourth-order tensor $\boldsymbol{C}^*$ is called *Hill's constraint tensor* and characterizes the stress acting on an inclusion by the infinite medium independently of the properties of the inclusion: $\boldsymbol{\sigma}_1 = -\boldsymbol{C}^* : \boldsymbol{\varepsilon}_1$. Tensor $\boldsymbol{C}^*$ possesses the minor symmetries by construction. In order to prove the major symmetries of this tensor, let's consider two different systems of loads (forces by unit of area) $F_i^{(1)}$ and $F_i^{(2)}$ acting of the interface inclusion/matrix of the single inclusion problem (figure 4.2b). These loads induce two different displacement fields, $u_i^{(1)}$ and

$u_i^{(2)}$, respectively. The Maxwell-Betti theorem gives the following equivalence of works:

$$\int_{\partial\omega} F_i^{(1)} u_i^{(2)} dS = \int_{\partial\omega} F_i^{(2)} u_i^{(1)} dS, \tag{4.15}$$

where $\partial\omega$ is the interface surface. By using the definition of the constraint tensor, expression (4.15) can be rewritten as:

$$\int_{\partial\omega} -C^*_{ijkl}\epsilon^{(1)}_{lk} n_j u_i^{(2)} dS = \int_{\partial\omega} -C^*_{ijkl}\epsilon^{(2)}_{lk} n_j u_i^{(1)} dS. \tag{4.16}$$

Since $\boldsymbol{C}^*$ has the minor symmetries, following relations hold:

$$\begin{aligned} \int_{\partial\omega} -C^*_{ijkl}\epsilon^{(1)}_{lk} n_j u_i^{(2)} dS &= \int_{\omega} -C^*_{ijkl}\epsilon^{(1)}_{lk} \frac{\partial u_i^{(2)}}{\partial x_j} dV \\ &= \int_{\omega} -C^*_{jikl}\epsilon^{(1)}_{lk} \frac{\partial u_j^{(2)}}{\partial x_i} dV. \end{aligned} \tag{4.17}$$

Expression (4.16) can be rewritten as:

$$\begin{aligned} \int_{\omega} C^*_{ijkl}\boldsymbol{\varepsilon}^{(1)}_{lk}\boldsymbol{\varepsilon}^{(2)}_{ij} dV &= \int_{\omega} C^*_{ijkl}\boldsymbol{\varepsilon}^{(2)}_{lk}\boldsymbol{\varepsilon}^{(1)}_{ij} \\ &= \int_{\omega} C^*_{klij}\boldsymbol{\varepsilon}^{(1)}_{lk}\boldsymbol{\varepsilon}^{(2)}_{ij} dV. \end{aligned} \tag{4.18}$$

Last relation is true for any load system $F^{(1)}$ and $F^{(2)}$. So, in order to satisfy this last relation, major symmetries are required:

$$C^*_{ijkl} = C^*_{klij}. \tag{4.19}$$

Consequently, $\boldsymbol{P}$ is also fully symmetric.

4.2.2 Expressions of localization tensors

In sections 2.1 and 2.2, the definition of a representative volume element has been given as well as a presentation of various boundary conditions to apply if either macroscopic stress or macroscopic strain is given. Localization expressions in linear elasticity are examined and resulting macroscopic relations are obtained accordingly. Developments in this section follow Zaoui [110].

Concentration tensors enable to link a local property to the corresponding macroscopic one. For example, given a macroscopic strain, the corresponding macroscopic stress writes:

$$\bar{\boldsymbol{\sigma}}(\bar{\varepsilon}) =< \boldsymbol{\sigma}(\boldsymbol{\varepsilon}(\boldsymbol{x})) >=< \boldsymbol{\sigma}(\boldsymbol{D}^{\varepsilon}(\boldsymbol{x}) : \bar{\varepsilon}) >, \tag{4.20}$$

where the strain concentration tensor $\boldsymbol{D}^{\varepsilon}$ relates the local strain at any point of the RVE to the macroscopic one:

$$\boldsymbol{\varepsilon}(x) = \boldsymbol{D}^{\varepsilon}(\boldsymbol{x}) : \bar{\boldsymbol{\varepsilon}}. \tag{4.21}$$

Each point of the RVE belongs to phase r whose behavior is given by a linear elastic relation as:

$$\boldsymbol{\sigma}(\boldsymbol{x}) = \boldsymbol{C}_r : \boldsymbol{\varepsilon}(\boldsymbol{x}), \tag{4.22}$$

where point $\boldsymbol{x}$ belongs to phase r of uniform stiffness $\boldsymbol{C}_r$.

For any heterogeneous material made of linear elastic constituents, the following macroscopic relation holds (proved by using the Hill's Lemma):

$$\bar{\boldsymbol{\sigma}} = \boldsymbol{C}^{\text{eff}} : \bar{\boldsymbol{\varepsilon}}, \tag{4.23}$$

where $\boldsymbol{C}^{eff}$ is the effective stiffness tensor. The macroscopic stress computed from the volume average of the stress microfield becomes:

$$\bar{\boldsymbol{\sigma}} =< \boldsymbol{\sigma}(\boldsymbol{x}) >=< \boldsymbol{C}_r : \boldsymbol{\varepsilon}(\boldsymbol{x}) >=< \boldsymbol{C}_r : \boldsymbol{D}^{\varepsilon}(\boldsymbol{x}) >: \bar{\boldsymbol{\varepsilon}} = \bar{\boldsymbol{C}} : \bar{\boldsymbol{\varepsilon}}. \tag{4.24}$$

Hypothesis on the strain concentration tensors $\boldsymbol{D}^{\boldsymbol{\varepsilon}}$ give a $\bar{\boldsymbol{C}}$ which is either an estimation or a bound of the effective stiffness $\boldsymbol{C}^{eff}$ and represents a macroscopically homogeneous material with an equivalent behavior to the one of the heterogeneous RVE.

4.2.3 Various homogenization schemes

In this section, a two-phase isothermal linear elastic composite with a uniform stiffness $\boldsymbol{C}_0$ for the matrix and $\boldsymbol{C}_1$ for the inclusions (subscript 0 always refers to the matrix and 1 to the inclusions) is considered . The RVE is subjected to linear boundary displacements corresponding to a macroscopic strain $\bar{\boldsymbol{\varepsilon}}$ so that per phase strain averages are related between each others and to $\bar{\boldsymbol{\varepsilon}}$ through a (still unknown) strain concentration tensor $\boldsymbol{B}^{\epsilon}$:

$$\begin{array}{cc} < \boldsymbol{\varepsilon} >_{\omega_1} = \boldsymbol{B}^{\epsilon} :< \boldsymbol{\varepsilon} >_{\omega_0} \quad , & < \boldsymbol{\varepsilon} >_{\omega_1} = \boldsymbol{A}^{\epsilon} : \bar{\boldsymbol{\varepsilon}}, \\ \boldsymbol{A}^{\epsilon} = \boldsymbol{B}^{\epsilon} : (v_1 \boldsymbol{B}^{\epsilon} + (1 - v_1)\boldsymbol{I})^{-1}, & \boldsymbol{B}^{\epsilon} = (1 - v_1)\boldsymbol{A}^{\epsilon} : (\boldsymbol{I} - v_1 \boldsymbol{A}^{\epsilon})^{-1}, \end{array} \tag{4.25}$$

where $\boldsymbol{I}$ designates the fourth-order symmetric identity tensor and $\boldsymbol{A}^{\epsilon}$ is the strain concentration tensor linking the average strain in the inclusions to the macroscopic one. For any homogenization model defined by $\boldsymbol{B}^{\boldsymbol{\varepsilon}}$, the macroscopic stiffness is given by:

$$\begin{aligned} \bar{\boldsymbol{C}} &= [v_1 \boldsymbol{C}_1 : \boldsymbol{B}^{\epsilon} + (1 - v_1)\boldsymbol{C}_0] : [v_1 \boldsymbol{B}^{\epsilon} + (1 - v_1)\boldsymbol{I}]^{-1} && (4.26) \\ &= [v_1 (\boldsymbol{C}^* + \boldsymbol{C}_1)^{-1} + (1 - v_1)(\boldsymbol{C}^* + \boldsymbol{C}_0)^{-1}]^{-1} - \boldsymbol{C}^*, && (4.27) \\ &= \boldsymbol{C}_0 + v_1 (\boldsymbol{C}_1 - \boldsymbol{C}_0) : \boldsymbol{A}^{\epsilon}. && (4.28) \end{aligned}$$

Since the Hill's constraint tensor $\boldsymbol{C}^*$ is fully symmetric, expression (4.27) imposes that the macroscopic tangent operator is also fully symmetric. This is a very important property since, as we will see in elasto-plastic simulations, some approximations of the matrix modulus might lead to the loss of major symmetries and finally give non physical results. Hypothesis on the strain concentration tensor defines an homogenization scheme so that the composite behavior can be predicted. On the contrary to basic models of Voigt and Reuss, more elaborated mean-field homogenization schemes rely on the solution of the Eshelby's problem. In addition to the volume fraction of each phase, they take into account of the shape and the orientation of the RVE constituents. However, due to the Eshelby's hypothesis, the inclusions must have an ellipsoidal shape as well as the same aspect ratio and orientation[2]. Otherwise, the composite is considered as a multi phase material (Pierard *et al.* [80]).

Voigt and Reuss models

Assuming a uniform strain within the RVE, the following results are immediately found:

$$\boldsymbol{B}^{\boldsymbol{\varepsilon}} = \boldsymbol{I}, \;\; \bar{\boldsymbol{C}} = v_1 \boldsymbol{C}_1 + (1 - v_1)\boldsymbol{C}_0. \tag{4.29}$$

This is known as the Voigt homogenization model and the effective moduli are thus the volume average of the per phase uniform local stiffnesses. Even with such a big approximation, the Voigt model gives good predictions in the longitudinal direction of materials reinforced by long fibers.

Another obvious hypothesis is to consider uniform stress within the RVE. Consequently, the following expressions are found:

$$\boldsymbol{B}^{\boldsymbol{\varepsilon}} = \boldsymbol{C}_1^{-1} : \boldsymbol{C}_0, \;\; \bar{\boldsymbol{C}} = \left[v_1 \boldsymbol{C}_1^{-1} + (1 - v_1)\boldsymbol{C}_0^{-1} \right]^{-1}. \tag{4.30}$$

This result is known as the Reuss homogenization model and the effective compliance is thus simply the volume average of the per phase uniform ones.

Mori-Tanaka model

The Mori-Tanaka model tries to take into account interactions between the inclusions. Since this model is intensively used in the numerical simulations of this work, derivation of the strain concentration tensor is briefly recalled.

Let's define a companion problem to the original one over the RVE in which the inclusions are made of the same material as the one of the matrix and undergo an eigenstrain $\boldsymbol{\varepsilon}^*$ (figure 4.3b). This fictitious material, as in the original problem, is subjected to linear displacements imposed at infinity which

[2]Note that we consider the same inclusion geometry in the original material and the associated single inclusion problem without taking into account the inclusions spatial distribution (see Bornert [11] and Ponte Castañeda and Willis [87] for more details).

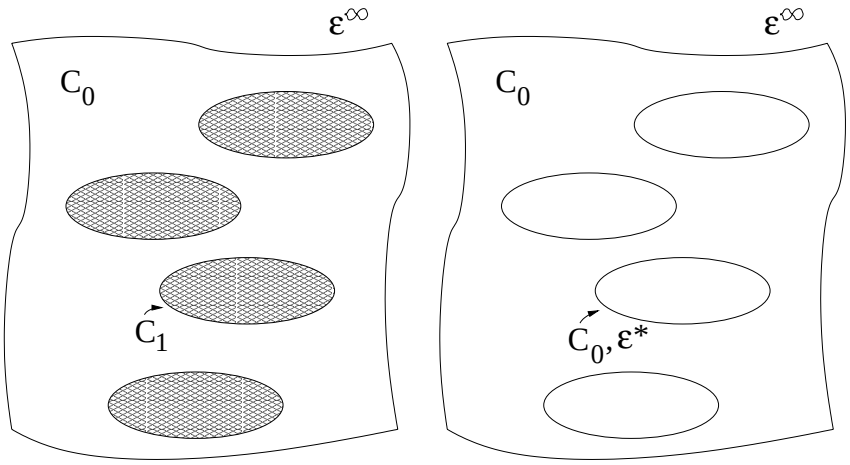

(a) Original problem. (b) Companion problem.

Figure 4.3: The two problems of the Mori-Tanaka homogenization scheme.

induce a uniform strain within both matrix and inclusions. With the help of the Eshelby's result and superposition principle, strain and stress in the inclusions of the companion problem are given by:

$$\boldsymbol{\varepsilon}_1 = \boldsymbol{\varepsilon}^{\infty} + \mathcal{E} : \boldsymbol{\varepsilon}^* + \boldsymbol{\varepsilon}^{'}(\boldsymbol{x}), \qquad \boldsymbol{\sigma}_1 = \boldsymbol{C}_0 : (\boldsymbol{\varepsilon}^{\infty} + \mathcal{E} : \boldsymbol{\varepsilon}^* + \boldsymbol{\varepsilon}^{'}(\boldsymbol{x}) - \boldsymbol{\varepsilon}^*), \quad (4.31)$$

where $\boldsymbol{\varepsilon}^{'}(\boldsymbol{x})$ is the sum of all the strain fields caused by the presence of each inclusion. Strain and stress equivalence in both phases between the companion and the original problem (inclusion's stiffness $\boldsymbol{C}_1$ and no eigenstrain, figure 4.3a) is satisfied if the same strain in the inclusions of both problems is imposed and:

$$\boldsymbol{C}_0 : (\boldsymbol{\varepsilon}^{\infty} + \mathcal{E} : \boldsymbol{\varepsilon}^* + \boldsymbol{\varepsilon}^{'}(\boldsymbol{x}) - \boldsymbol{\varepsilon}^*) = \boldsymbol{C}_1 : (\boldsymbol{\varepsilon}^{\infty} + \mathcal{E} : \boldsymbol{\varepsilon}^* + \boldsymbol{\varepsilon}^{'}(\boldsymbol{x})). \quad (4.32)$$

Such condition cannot be fulfilled at each point of the material. However, a solution exists if an average over all the inclusions is considered:

$$\boldsymbol{C}_0 : (\boldsymbol{\varepsilon}^{\infty} + \mathcal{E} : \boldsymbol{\varepsilon}^* + < \boldsymbol{\varepsilon}^{'}(\boldsymbol{x}) >_{\omega_1} - \boldsymbol{\varepsilon}^*) = \boldsymbol{C}_1 : (\boldsymbol{\varepsilon}^{\infty} + \mathcal{E} : \boldsymbol{\varepsilon}^* + < \boldsymbol{\varepsilon}^{'}(\boldsymbol{x}) >_{\omega_1}).$$

Equivalence is fulfilled for the following expression of the eigenstrain:

$$\boldsymbol{\varepsilon}^* = -\left[(\boldsymbol{C}_0^{-1} : \boldsymbol{C}_1 - \boldsymbol{I})^{-1} + \mathcal{E}\right]^{-1} : (\boldsymbol{\varepsilon}^{\infty} + < \boldsymbol{\varepsilon}^{'}(\boldsymbol{x}) >_{\omega_1}). \quad (4.33)$$

Combining this expression with the one of the average strain in the inclusions gives:

$$< \boldsymbol{\varepsilon} >_{\omega_1} = \left[\boldsymbol{I} - \mathcal{E} : \left((\boldsymbol{C}_0^{-1} : \boldsymbol{C}_1 - \boldsymbol{I})^{-1} + \mathcal{E}\right)^{-1}\right] : (\boldsymbol{\varepsilon}^{\infty} + < \boldsymbol{\varepsilon}^{'}(\boldsymbol{x}) >_{\omega_1}). \quad (4.34)$$

This expression is valid if Eshelby's tensor is the same for all the inclusions, i.e. all the inclusions are similarly shaped and aligned. Due to the infinite number of inclusions randomly dispersed in the RVE, we can say that the disturbance field $\boldsymbol{\varepsilon}'(\boldsymbol{x})$ is, on average, the same in the inclusions and in the matrix so that average strain in the matrix can be rewritten as:

$$< \boldsymbol{\varepsilon} >_{\omega_0} = \boldsymbol{\varepsilon}^{\infty} + < \boldsymbol{\varepsilon}'(\boldsymbol{x}) >_{\omega_0} = \boldsymbol{\varepsilon}^{\infty} + < \boldsymbol{\varepsilon}'(\boldsymbol{x}) >_{\omega_1} . \tag{4.35}$$

Inserting this result into (4.34), expression of the strain concentration tensor linking the average strain in the inclusion to the one in the matrix is given by:

$$\begin{aligned} \boldsymbol{B}^{\epsilon} &= [\boldsymbol{I} + \mathcal{E} : (\boldsymbol{C}_0^{-1} : \boldsymbol{C}_1 - \boldsymbol{I})]^{-1} = \boldsymbol{B}_{\text{M-T}}(\boldsymbol{C}_0, \boldsymbol{C}_1) \\ &= [\boldsymbol{I} + \boldsymbol{P} : (\boldsymbol{C}_1 - \boldsymbol{C}_0)]^{-1} \qquad (4.36) \\ &= (\boldsymbol{C}^* + \boldsymbol{C}_1)^{-1} : (\boldsymbol{C}^* + \boldsymbol{C}_0). \qquad (4.37) \end{aligned}$$

This is the same result as the one obtained for a matrix reinforced by a single inclusion undergoing uniform strain at infinity. Consequently, Benveniste [7] proposed the following interpretation: "each inclusion behaves like an isolated inclusion in the matrix seeing $< \boldsymbol{\varepsilon} >_{\omega_0}$ as a far-field strain". The Mori-Tanaka model is particularly suitable for particle reinforced composite materials up to moderate volume fractions (25-30%).

For higher volume fractions, Lielens [62] proposed an extension of this model which combines a nonlinear interpolation between the original Mori-Tanaka model and the one considering reverse material properties (which corresponds to the second Hashin-Shtrikman-Willis bound [107], see section 4.2.4). The strain concentration tensor then reads:

$$\boldsymbol{B}^{\epsilon} = \left[(1 - f(v_1))\boldsymbol{B}_{\text{M-T}}^{-1}(\boldsymbol{C}_0, \boldsymbol{C}_1) + f(v_1)\boldsymbol{B}_{\text{M-T}}(\boldsymbol{C}_1, \boldsymbol{C}_0)\right]^{-1} . \tag{4.38}$$

The proposed interpolative function is $f(v_1) = (v_1 + v_1^2)/2$. This homogenization scheme is called Lielens' *interpolative model*.

Self-consistent model

The self-consistent model (S-C) assumes that each inclusion is isolated and embedded in a fictitious homogeneous matrix possessing the composite's unknown stiffness $\bar{\boldsymbol{C}}$ seeing $\bar{\boldsymbol{\varepsilon}}$ as a far-field strain. This problem thus becomes similar to the one of the single inclusion problem and the strain concentration reads:

$$< \boldsymbol{\varepsilon} >_{\omega_1} = \boldsymbol{B}_{\text{M-T}}(\bar{\boldsymbol{C}}, \boldsymbol{C}_1) : \bar{\boldsymbol{\varepsilon}} = \boldsymbol{A}^{\epsilon}(\bar{\boldsymbol{C}}, \boldsymbol{C}_1) : \bar{\boldsymbol{\varepsilon}}. \tag{4.39}$$

The localization problem becomes implicit ($\bar{\boldsymbol{C}}$ is computed from the strain concentration tensor $\boldsymbol{A}^{\epsilon}$, see (4.28)) and requires an additional iterative loop in order to determine $\bar{\boldsymbol{C}}$. Strain concentration tensors are given by:

$$\boldsymbol{B}^{\epsilon} = (1 - v_1)\boldsymbol{A}^{\epsilon} : (\boldsymbol{I} - v_1\boldsymbol{A}^{\epsilon})^{-1}, \qquad \boldsymbol{A}^{\epsilon} = \left[\boldsymbol{I} + \mathcal{E} : (\bar{\boldsymbol{C}}^{-1} : \boldsymbol{C}_1 - \boldsymbol{I})\right]^{-1} . \tag{4.40}$$

The self-consistent model generally gives good predictions for polycrystals but is less satisfying in the case of two-phase composites.

4.2.4 Some bounds

All the previous models give estimates for the effective moduli of the equivalent homogeneous material. However, given information on the phase modulus and geometry of the microstructure, bounds can be derived from the minimum principle for elastic media. Following Zaoui [110], if linear displacement boundary conditions are imposed, among all the strain fields $\boldsymbol{\varepsilon}^*$ which satisfy these conditions, the average microscopic work of the real solution $\boldsymbol{\varepsilon}$ to the boundary value problem is always smaller (position dependence is omitted for clarity):

$$< \boldsymbol{\varepsilon}^* : \boldsymbol{C} : \boldsymbol{\varepsilon}^* > \geq < \boldsymbol{\varepsilon} : \boldsymbol{C} : \boldsymbol{\varepsilon} > . \tag{4.41}$$

Similarly, if uniform tractions are imposed, this reads:

$$< \boldsymbol{\sigma}^* : \boldsymbol{S} : \boldsymbol{\sigma}^* > \geq < \boldsymbol{\sigma} : \boldsymbol{S} : \boldsymbol{\sigma} > . \tag{4.42}$$

Making use of Hill's lemma and introducing the strain concentration tensor $\boldsymbol{D}^{\boldsymbol{\varepsilon}}$ ($\boldsymbol{\varepsilon}^*(x) = \boldsymbol{D}^{\boldsymbol{\varepsilon}}(\boldsymbol{x}) : \bar{\boldsymbol{\varepsilon}}$) and the stress concentration tensor $\boldsymbol{D}^{\sigma}$ ($\boldsymbol{\sigma}^*(x) = \boldsymbol{D}^{\sigma}(\boldsymbol{x}) : \bar{\boldsymbol{\sigma}}$), these two equations can be rewritten as:

$$\begin{aligned} \bar{\boldsymbol{\varepsilon}} : (< \boldsymbol{D}^{\varepsilon^T} : \boldsymbol{C} : \boldsymbol{D}^{\varepsilon} > - \boldsymbol{C}^{eff}) : \bar{\boldsymbol{\varepsilon}} &\geq 0 \qquad \forall \bar{\boldsymbol{\varepsilon}}, \\ \bar{\boldsymbol{\sigma}} : (< \boldsymbol{D}^{\sigma^T} : \boldsymbol{S} : \boldsymbol{D}^{\sigma} > - \boldsymbol{S}^{eff}) : \bar{\boldsymbol{\sigma}} &\geq 0 \qquad \forall \bar{\boldsymbol{\sigma}}. \end{aligned} \tag{4.43}$$

From these expressions, bounds can be derived. A basic hypothesis is to consider a uniform strain field which respects linear displacement boundary conditions. This leads to the Voigt bound on the effective moduli:

$$\bar{\boldsymbol{\varepsilon}} : (< \boldsymbol{C} > - \boldsymbol{C}^{eff}) : \bar{\boldsymbol{\varepsilon}} \geq 0 \qquad \forall \bar{\boldsymbol{\varepsilon}}. \tag{4.44}$$

Similarly, for a uniform stress field which respects uniform traction boundary conditions, the Reuss bound is found:

$$\bar{\boldsymbol{\sigma}} : (< \boldsymbol{S} > - \boldsymbol{S}^{eff}) : \bar{\boldsymbol{\sigma}} \geq 0 \qquad \forall \bar{\boldsymbol{\sigma}}. \tag{4.45}$$

If materials are isotropic, these relations can be reduced to much more interesting bounds on the effective shear (μ^{eff}) and bulk (κ^{eff}) moduli:

$$< \mu^{-1} >^{-1} \leq \mu^{eff} \leq < \mu >, \qquad < \kappa^{-1} >^{-1} \leq \kappa^{eff} \leq < \kappa > . \tag{4.46}$$

Voigt/Reuss bounds can be improved, as shown in Hashin and Shtrikman [38] for overall isotropic materials. This was later extended to anisotropic constituents, anisotropic phase arrangements and/or aligned non spherical arrangements (Walpole [102], Willis [107]). In general, the Mori-Tanaka estimate

correspond to one of the extended Hashin-Shtrikman bounds for two-phase materials (Weng [105]). The other one can be obtained with a Mori-Tanaka estimate of a fictitious material with reverse material properties. Better bounds have been developed, but this requires additional hypotheses on the geometry (Bornert *et al.* [12], Hervé and Zaoui [39, 40]). A more recent work which gives very close bounds is the second-order method of Torquato [99].

4.3 Homogenization of thermo-elastic composites

4.3.1 Homogenization technique

Consider a two-phase composite, where the matrix has uniform properties $\boldsymbol{C}_0$ and $\boldsymbol{\alpha}_0$, and the inclusions have the same aspect ratio, orientation and properties $\boldsymbol{C}_1$ and $\boldsymbol{\alpha}_1$. Relations (4.1-4.3) hold for each phase; our aim is to write similar macroscopic relations for the whole composite. In order to determine the macroscopic properties $\bar{\boldsymbol{C}}$ and $\bar{\boldsymbol{\alpha}}$, one can re-derive a homogenization model taking into account thermo-elastic behavior instead of isothermal elasticity. A better alternative is proposed in Lielens [61]. Its major interest is that given any homogenization model which is defined in the isothermal case by its strain concentration tensor $\boldsymbol{B}^\epsilon$ (or $\boldsymbol{A}^\epsilon$), general expressions of the macroscopic thermo-elastic properties can be found [3]. For this, linear displacement boundary conditions corresponding to a macroscopic total strain $\bar{\boldsymbol{\varepsilon}} =< \boldsymbol{\varepsilon} >$ and uniform temperature change ΔT are assumed. The proof is based on the following three-step approach.

First step

In this step, the composite is subjected to linear boundary displacements corresponding to the final total strain $\boldsymbol{\varepsilon}^{s1} = \bar{\boldsymbol{\varepsilon}}$ and to zero change in temperature $\Delta T^{s1} = 0$. This step corresponds to a classical isothermal transformation whose solution is given in section 4.2.3. The per phase strain averages are found as follows:

$$< \boldsymbol{\varepsilon}^{s1} >_{\omega_1} = \boldsymbol{A}^\epsilon : \bar{\boldsymbol{\varepsilon}}, \qquad v_1 < \boldsymbol{\varepsilon}^{s1} >_{\omega_1} + (1 - v_1) < \boldsymbol{\varepsilon}^{s1} >_{\omega_0} = \bar{\boldsymbol{\varepsilon}}, \tag{4.47}$$

where $\boldsymbol{A}^\epsilon$ is given by equation (4.25) and its expression depends on the chosen homogenization model. The stress averages are given by:

$$< \boldsymbol{\sigma}^{s1} >_{\omega_1} = \boldsymbol{C}_1 :< \boldsymbol{\varepsilon}^{s1} >_{\omega_1}, \qquad < \boldsymbol{\sigma}^{s1} >_{\omega_0} = \boldsymbol{C}_0 :< \boldsymbol{\varepsilon}^{s1} >_{\omega_0} . \tag{4.48}$$

[3] An alternative if the macroscopic stiffness is known consists of using the Levin's theorem [55]: $\bar{\boldsymbol{\beta}} = ((1 - v_1)\boldsymbol{\beta}_0 + v_1\boldsymbol{\beta}_1) + (\bar{\boldsymbol{C}} - (1 - v_1)\boldsymbol{\beta}_0 - v_1\boldsymbol{\beta}_1) : (\boldsymbol{C}_1 - \boldsymbol{C}_0)^{-1} : (\boldsymbol{\beta}_1 - \boldsymbol{\beta}_0)$.

Second step

In this step, the RVE witnesses a uniform temperature increment equal to the final temperature change $\Delta T^{s2} = \Delta T$, and incremental boundary linear displacements corresponding to a macroscopic strain increment $\Delta\bar{\boldsymbol{\varepsilon}}^{s2}$ are imposed so that uniform strain and stress increments are obtained:

$$\Delta\boldsymbol{\sigma}^{s2} = \boldsymbol{C}_0 : \Delta\bar{\boldsymbol{\varepsilon}}^{s2} + \boldsymbol{\beta}_0\Delta T = \boldsymbol{C}_1 : \Delta\bar{\boldsymbol{\varepsilon}}^{s2} + \boldsymbol{\beta}_1\Delta T. \tag{4.49}$$

This allows to compute the uniform total strain increment:

$$\Delta\bar{\epsilon}^{s2} = -(\boldsymbol{C}_1 - \boldsymbol{C}_0)^{-1} : (\boldsymbol{\beta}_1 - \boldsymbol{\beta}_0)\Delta T. \tag{4.50}$$

Third step

In this step, the composite is subjected to linear boundary displacements corresponding to a macroscopic total strain increment $\Delta\bar{\boldsymbol{\varepsilon}}^{s3}$ and to zero temperature increment $\Delta T^{s3} = 0$. This is a classical isothermal transformation whose solution is given in section 4.2.3 as follows:

$$< \Delta\boldsymbol{\varepsilon}^{s3} >_{\omega_1} = \boldsymbol{A}^{\epsilon} : \Delta\bar{\boldsymbol{\varepsilon}}^{s3}, \qquad v_1 < \Delta\boldsymbol{\varepsilon}^{s3} >_{\omega_1} + (1 - v_1) < \Delta\boldsymbol{\varepsilon}^{s3} >_{\omega_0} = \Delta\bar{\boldsymbol{\varepsilon}}^{s3},$$

where $\boldsymbol{A}^{\epsilon}$ is given by equation (4.25). The per-phase stress averages are given by:

$$< \Delta\boldsymbol{\sigma}^{s3} >_{\omega_1} = \boldsymbol{C}_1 :< \Delta\boldsymbol{\varepsilon}^{s3} >_{\omega_1}, \qquad < \Delta\boldsymbol{\sigma}^{s3} >_{\omega_0} = \boldsymbol{C}_0 :< \Delta\boldsymbol{\varepsilon}^{s3} >_{\omega_0} . \tag{4.51}$$

Superposition

Using the superposition theorem, it is seen that at the end of the three steps, the per-phase strain averages are given by:

$$< \boldsymbol{\varepsilon} >_{\omega_1} = \boldsymbol{A}^{\epsilon} : (\bar{\boldsymbol{\varepsilon}} + \Delta\bar{\boldsymbol{\varepsilon}}^{s3}) + \Delta\bar{\boldsymbol{\varepsilon}}^{s2} \tag{4.52}$$

$$v_1 < \boldsymbol{\varepsilon} >_{\omega_1} + (1 - v_1) < \boldsymbol{\varepsilon} >_{\omega_0} = \bar{\boldsymbol{\varepsilon}} + \Delta\bar{\boldsymbol{\varepsilon}}^{s2} + \Delta\bar{\boldsymbol{\varepsilon}}^{s3}, \tag{4.53}$$

where $\Delta\bar{\boldsymbol{\varepsilon}}^{s2}$ is given by equation (4.50). At the end of the three steps, the RVE is subjected to a uniform temperature change ΔT and linear boundary displacements corresponding to a macroscopic total strain $\bar{\boldsymbol{\varepsilon}} + \Delta\bar{\boldsymbol{\varepsilon}}^{s2} + \Delta\bar{\boldsymbol{\varepsilon}}^{s3}$. However, the latter value should be equal to $\bar{\boldsymbol{\varepsilon}}$, therefore we have:

$$\Delta\bar{\boldsymbol{\varepsilon}}^{s3} = -\Delta\bar{\boldsymbol{\varepsilon}}^{s2}. \tag{4.54}$$

Consequently, the per-phase strain averages can be computed from equations (4.50) and (4.52-4.53), the per-phase stress averages from equations (4.48 - 4.49) and (4.51), and the stress average over the RVE by superposition,

$$\begin{aligned} < \boldsymbol{\sigma} > = \Delta\boldsymbol{\sigma}^{s2} + (1 - v_1) \left(< \boldsymbol{\sigma}^{s1} >_{\omega_0} + < \Delta\boldsymbol{\sigma}^{s3} >_{\omega_0} \right), \\ + v_1 \left(< \boldsymbol{\sigma}^{s1} >_{\omega_1} + < \Delta\boldsymbol{\sigma}^{s3} >_{\omega_1} \right). \end{aligned} \tag{4.55}$$

Final expressions

Carrying out the computations and rearranging terms, the following expressions for the total strain averages are found:

$$< \boldsymbol{\varepsilon} >_{\omega_1} = \boldsymbol{A}^{\epsilon} : \bar{\boldsymbol{\varepsilon}} + \boldsymbol{a}^{\epsilon} \Delta T,$$
$$\boldsymbol{a}^{\epsilon} = (\boldsymbol{A}^{\epsilon} - \boldsymbol{I}) : (\boldsymbol{C}_1 - \boldsymbol{C}_0)^{-1} : (\boldsymbol{\beta}_1 - \boldsymbol{\beta}_0), \tag{4.56}$$
$$v_1 < \boldsymbol{\varepsilon} >_{\omega_1} + (1 - v_1) < \boldsymbol{\varepsilon} >_{\omega_0} = \bar{\boldsymbol{\varepsilon}}, \tag{4.57}$$

where $\boldsymbol{A}^{\epsilon}$ is defined in equation (4.25). Similarly to (4.2), it is found that the macroscopic thermo-elastic response is written under the following format:

$$< \boldsymbol{\sigma} > = \bar{\boldsymbol{C}} : \bar{\boldsymbol{\varepsilon}} + \bar{\boldsymbol{\beta}} \, \Delta T; \qquad \bar{\boldsymbol{\beta}} = (1 - v_1)\beta_0 + v_1 \boldsymbol{\beta}_1 + v_1 (\boldsymbol{C}_1 - \boldsymbol{C}_0) : \boldsymbol{a}^{\epsilon}, \tag{4.58}$$

where the macroscopic stiffness $\bar{\boldsymbol{C}}$ is given by the isothermal expression (4.26), $\boldsymbol{a}^{\epsilon}$ by equation (4.56) and the macroscopic thermal expansion $\bar{\boldsymbol{\alpha}}$ is defined as follows:

$$\bar{\boldsymbol{\alpha}} = -\bar{\boldsymbol{C}}^{-1} : \bar{\beta}. \tag{4.59}$$

In conclusion, generic expressions for thermo-elastic properties are obtained for any homogenization model defined in the isothermal case by its strain concentration tensor $\boldsymbol{B}^{\boldsymbol{\varepsilon}}$ (or equivalently $\boldsymbol{A}^{\epsilon}$).

Special case.

When the two phases have identical stiffness operators ($\boldsymbol{C}_0 = \boldsymbol{C}_1 \equiv \boldsymbol{C}$), equations (4.56) and (4.58) become invalid. Lielens [61] suggests the following solution. In the previous three-step method, step 1 remains unchanged and steps 2 and 3 are replaced by one single step in which the RVE is subjected to a uniform temperature change $\Delta T^{s2} = \Delta T$ and zero boundary displacements corresponding to zero macroscopic total strain $\Delta \bar{\boldsymbol{\varepsilon}}^{s2} = 0$. The average stress is then:

$$\begin{aligned} < \Delta \boldsymbol{\sigma}^{s2} > &= (1 - v_1) < \boldsymbol{C} : \Delta \boldsymbol{\varepsilon}^{s2} + \boldsymbol{\beta}_0 \Delta T >_{\omega_0} \\ &\quad + v_1 < \boldsymbol{C} : \Delta \boldsymbol{\varepsilon}^{s2} + \boldsymbol{\beta}_1 \Delta T >_{\omega_1} \\ &= \boldsymbol{C} : \Delta \bar{\boldsymbol{\varepsilon}}^{s2} + [(1 - v_1)\boldsymbol{\beta}_0 + v_1 \boldsymbol{\beta}_1] \Delta T \\ &= ((1 - v_1)\boldsymbol{\beta}_0 + v_1 \boldsymbol{\beta}_1) \Delta T. \end{aligned} \tag{4.60}$$

Superposition of steps 1 and 2 shows then that:

$$< \boldsymbol{\sigma} > = \bar{\boldsymbol{C}} : \bar{\boldsymbol{\varepsilon}} + \bar{\boldsymbol{\beta}} \, \Delta T; \;\; \bar{\boldsymbol{\beta}} = (1 - v_1)\beta_0 + v_1 \boldsymbol{\beta}_1. \tag{4.61}$$

where the macroscopic stiffness $\bar{\boldsymbol{C}}$ is given by the isothermal expression (4.26).

4.3.2 Numerical simulations

In this section, macroscopic predictions are compared with experimental data and FE results obtained either on a RVE or a unit cell.

Influence of the inclusion's shape

Consider a thermo-elastic composite made of a polymer matrix ($E_0 = 3.0$ GPa, $\nu_0 = 0.35$ and $\alpha_0 = 70 \times 10^{-6}\, K^{-1}$) reinforced with aligned inclusions ($E_1 = 172.0$ GPa, $\nu_1 = 0.2$ and $\alpha_1 = 10^{-6}\, K^{-1}$). Notice the high contrast between Young's moduli and CTEs. A uniaxial traction test is simulated in the direction of the revolution axis of the inclusions.

M-T predictions of the CTE are confronted with those of van Es [101]. The latter model is based on a simplified two-phase composite which is a superposition of a layer made of the matrix material and another one made of the inclusions material. The interaction between the inclusions is thus not directly taken into account. However, in this formulation appears the homogenized stiffness tensor of linear elasticity which might be calculated previously through a classical M-T approach. Results of the predictions of the macroscopic CTE in the longitudinal direction are reported on figure 4.4 for various volume fractions of the inclusions and various aspect ratios. Both methods give very similar results. Logically, since the matrix has a higher CTE than the inclusions, the longitudinal CTE will be higher for platelets (i.e. small Ar) than for fibers (i.e. high Ar).

Comparison of various predictive methods

Short glass fiber reinforced composite is now considered ($E_1 = 72.5$ GPa, $\nu_1 = 0.2$, $\alpha_1 = 4.9 \times 10^{-6}\, K^{-1}$, $A_r = 35.58$ and $v_1 = 8\%$). The matrix characteristics are: $E_0 = 1.57$ GPa, $\nu_0 = 0.335$ and $\alpha_0 = 108.3 \times 10^{-6}\, K^{-1}$.

A uniaxial tension test is performed in a direction aligned with the fibers. Predictions with the M-T and interpolative models of the macroscopic longitudinal and transverse Young's moduli and CTE are confronted with experimental data found in Lusti *et al.* [65]. In that paper, several simplified methods are also used and recalled hereafter. McCullough's model predicts the macroscopic characteristics directly. Two microscopic approaches were proposed by Takao and Taya [98]. The first one is a simple second order average of the longitudinal and transverse CTE (noted hereafter Takao-Taya/aggregate). The second one, proposed by Tandon and Weng tried to include elastic constraints. This approach is noted Tandon-Weng/laminate hereafter. Comparison of all these approaches with our mean-field homogenization predictions of the macroscopic properties is reported in table 4.1. Note that for the predictions made with homogenization schemes, aspect ratios of the fibers are multiplied by 1.25 in order to try to model the cylinders by spheroids, as proposed by Li and Ponte

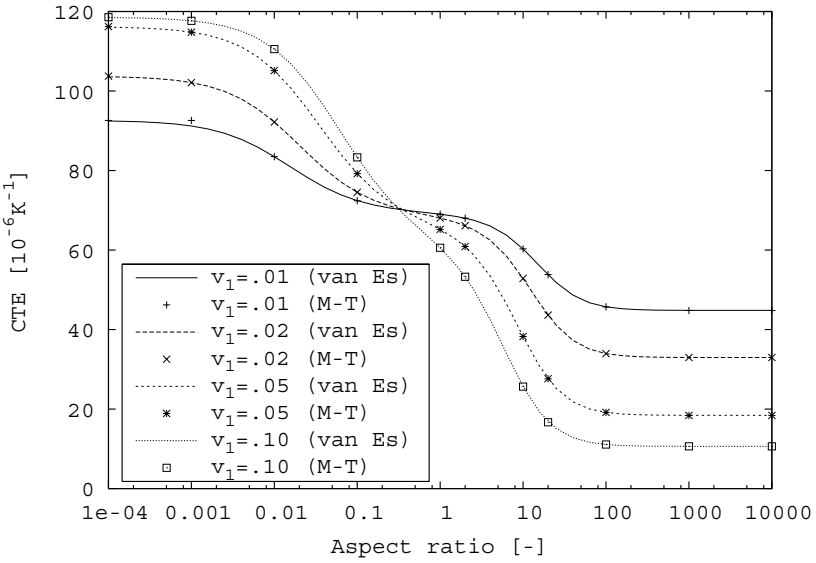

Figure 4.4: Influence of the aspect ratio on the macroscopic thermal expansion coefficient for different volume fractions of a linear thermo-elastic composite.

Castañeda [57]. Table 4.1 shows that our predictions with both homogenization models are very close to experimental results and this generally leads to slightly better predictions than with simplified models. These predictions also agree with Palmyra [75] 3D FE results (using first-order tetrahedra and periodic boundary conditions) while our procedure is much less time-consuming.

Transversely isotropic inclusions

A graphite fiber-reinforced composite is now considered. The main difference with the previous cases is that the inclusion's material is not isotropic anymore but transversely isotropic (subscript L denotes the longitudinal direction -the one of anisotropy- and T a transverse one). A slight modification of the method in order to take into account this particularity is proposed hereafter.

Since Eshelby's tensor only depends on the matrix properties and the shape of the inclusions, it will not be modified when used in M-T. However, when storing the tensors (accordingly with the traditional storage of strain and stress tensors[4]), stiffness matrix and the thermal expansion vector must be written

[4] $[\boldsymbol{\sigma}] = [\sigma_{11} \quad \sigma_{22} \quad \sigma_{33} \quad \sigma_{23} \quad \sigma_{13} \quad \sigma_{12}]^T$, $[\boldsymbol{\varepsilon}] = [\varepsilon_{11} \quad \varepsilon_{22} \quad \varepsilon_{33} \quad 2\varepsilon_{23} \quad 2\varepsilon_{13} \quad 2\varepsilon_{12}]^T$

Model	$\bar{E}_L$ [GPa]	$\bar{E}_T$ [GPa]	$\bar{\boldsymbol{\alpha}}_L$ [$10^{-6}\mathrm{K}^{-1}$]	$\bar{\boldsymbol{\alpha}}_T$ [$10^{-6}\mathrm{K}^{-1}$]
Experiment [65]	5.99		27.7 ± 1.7	121 ± 1
M-T	6.097	1.929	30.1	120.6
M-T($A_r \times 1.25$)	6.401	1.932	28.9	121.0
Interpol. model	6.136	1.938	30.0	120.1
Interpol. model ($A_r \times 1.25$)	6.432	1.941	28.8	120.5
FE [65]			29.3 ± 0.1	119 ± 0.1
Takao-Taya/aggregate [65]			32.0	120
Tandon-Weng/laminate [65]			29.4	119
McCullough [65]	< 5.89		31.4	121

Table 4.1: Short glass fiber reinforced composite: predictions of the macroscopic thermo-mechanical properties by using various homogenization schemes and comparison with several predictive formulae [65].

under the following form, using the direction 1 as the direction of the aligned fibers:

$$\boldsymbol{C}_1 = \begin{pmatrix} \frac{1}{E_L} & -\frac{\nu_{LT}}{E_T} & -\frac{\nu_{LT}}{E_L} & 0 & 0 & 0 \\ -\frac{\nu_{LT}}{E_T} & \frac{1}{E_T} & -\frac{\nu_T}{E_T} & 0 & 0 & 0 \\ -\frac{\nu_{LT}}{E_L} & -\frac{\nu_T}{E_T} & \frac{1}{E_T} & 0 & 0 & 0 \\ 0 & 0 & 0 & \frac{2(1+\nu_T)}{E_T} & 0 & 0 \\ 0 & 0 & 0 & 0 & \frac{1}{\mu_{LT}} & 0 \\ 0 & 0 & 0 & 0 & 0 & \frac{1}{\mu_{LT}} \end{pmatrix}^{-1},$$

$$\boldsymbol{\alpha}_1 = \begin{pmatrix} \alpha_L & \alpha_T & \alpha_T & 0 & 0 & 0 \end{pmatrix}^T.$$

For this test, two materials are considered for the matrix: 930/934 epoxy ($E_0 = 0.63$ GPa, $\nu_0 = 0.37$ and $\alpha_0 = 24.4 \times 10^{-6}$ K^{-1}) and PMR15 polyimide ($E_0 = 0.50$ GPa, $\nu_0 = 0.35$ and $\alpha_0 = 20.0 \times 10^{-6}$ K^{-1}), and two kinds of graphite fibers: C6000 ($E_{1,L} = 33.8$ GPa, $E_{1,T} = 3.35$ GPa, $\mu_{1,LT} = 1.30$ GPa, $\nu_{1,LT} = 0.20$, $\nu_{1,T} = 0.40$ and $A_{r_1} = \infty$) and P75 ($E_{1,L} = 79.8$ GPa, $E_{1,T} = 1.38$ GPa, $\mu_{1,LT} = 1.00$ GPa, $\nu_{1,LT} = 0.20$, $\nu_{1,T} = 0.40$ and $A_{r_1} = \infty$) where $-\nu_{LT}$ represents the ratio of the strain in the transverse direction over the strain in the longitudinal direction in a uniaxial tension test along the fibers. Predictions by using the M-T homogenization scheme are confronted to several experimental results, some well-known analytical predictions for the CTE and FE results assuming generalized plane strain on square and hexagonal arrays of fibers (Bowles and Tompkins [13]). These are reported in table 4.2. Note that the Schapery's predictive formula, which exists for the longitudinal and transverse directions, is only valid for isotropic constituents and so it does not

Composite - CTE	Exp.	FE (Hex)	FE (Sq)	M-T	SH	RH
P75/934 - $\bar{\alpha}_L$	-0.584	-0.512	-0.512	-0.512	-0.537	-0.512
P75/934 - $\bar{\alpha}_T$	19.18	19.07	19.06	18.92	19.70	18.90
P75/930 - $\bar{\alpha}_L$	-0.598	-0.627	-0.625	-0.627	-0.644	-0.627
P75/930 - $\bar{\alpha}_T$	17.62	14.04	14.00	13.90	14.80	13.90
C6000/PMR15 - $\bar{\alpha}_L$	-0.118	-0.104	-0.099	-0.104	-0.125	-0.104
C6000/PMR15 - $\bar{\alpha}_T$	12.46	12.56	12.36	12.54	14.30	12.40

Table 4.2: Transversely isotropic graphite fibers-reinforced composites: prediction of the longitudinal and transverse macroscopic CTE ($[10^{-6}\mathrm{K}^{-1}]$) with direct predictive formulae [13] (Shapery (SH), Rosen and Hashin (RH)), FE on a hexagonal (Hex) or square (Sq) fibers arrangement [13], homogenization scheme (M-T) and experimental results (Exp.). Volume fraction of fibers are: 0.48 for P75/934, 0.65 for P75/930 and 0.63 for C6000/PMR15.

account for the different values of the CTE of the inclusions in different directions. Good predictions are observed with mean-field homogenization schemes, especially for the transverse macroscopic CTE which is much more dependent on the predictive technique used.

4.4 Homogenization of viscoelastic composites

4.4.1 Homogenization technique

Consider a two-phase linear viscoelastic composite, each phase obeying a constitutive law of the form (4.6/4.7). By using the Laplace-Carson transform (see appendix B.1), the convolution product becomes a single contraction without rate dependence anymore so that constitutive laws can be rewritten in the Laplace domain as:

$$\begin{aligned} \boldsymbol{\sigma}^*(s) &= \boldsymbol{G}^*(s) : \boldsymbol{\varepsilon}^*(s), \\ \text{or equivalently } \boldsymbol{\varepsilon}^*(s) &= \boldsymbol{J}^*(s) : \boldsymbol{\sigma}^*(s), \\ \text{with } \boldsymbol{G}^*(s) &= \left[\boldsymbol{J}^*(s)\right]^{-1}. \end{aligned} \tag{4.62}$$

These equations are similar to those of linear isothermal elasticity. Of course, they are fictitious constitutive equations since they are defined in the Laplace-Carson domain. However, one can apply the homogenization schemes valid in linear isothermal elasticity in order to obtain the homogenized modulus $\bar{\boldsymbol{G}}^*$ or

$\bar{\boldsymbol{J}}^*$:

$$\begin{aligned} \bar{\boldsymbol{\sigma}}^*(s) &= \bar{\boldsymbol{G}}^*(s) : \bar{\boldsymbol{\varepsilon}}^*(s), \\ \text{or equivalently } \bar{\boldsymbol{\varepsilon}}^*(s) &= \bar{\boldsymbol{J}}^*(s) : \bar{\boldsymbol{\sigma}}^*(s), \\ \text{with } \bar{\boldsymbol{G}}^*(s) &= \left[\bar{\boldsymbol{J}}^*(s)\right]^{-1}. \end{aligned} \tag{4.63}$$

Using a numerical inversion of the Laplace-Carson transform (see appendix B.2) to find the corresponding time dependent operators, the following expressions enable to compute the macroscopic response:

$$\begin{aligned} \bar{\boldsymbol{\sigma}}(t) &= \bar{\boldsymbol{G}}(t) : \bar{\boldsymbol{\varepsilon}}(0) + \int_0^t \bar{\boldsymbol{G}}(t-\tau) : \dot{\bar{\boldsymbol{\varepsilon}}}(\tau) d\tau, \\ \bar{\boldsymbol{\varepsilon}}(t) &= \bar{\boldsymbol{J}}(t) : \bar{\boldsymbol{\sigma}}(0) + \int_0^t \bar{\boldsymbol{J}}(t-\tau) : \dot{\bar{\boldsymbol{\sigma}}}(\tau) d\tau. \end{aligned} \tag{4.64}$$

For the numerical inversion, the use of 20 collocation points is recommended. Those are chosen as equispaced on a logarithmic scale containing at least all the relaxation times of the homogeneous materials. If the relaxation functions of the phases are particularly simple, a lower number of points may be considered (5 to 10).

4.4.2 Numerical simulations

As seen later in this work, homogenization of linear viscoelastic composites is a subproblem of the affine formulation developed for homogenization of elasto-viscoplastic composites. Accuracy of this subproblem is thus of first importance. As basic validation for homogenization of linear viscoelastic composites, the following material defined by Prony series is considered. Time dependent Young's modulus of the matrix is $E_0 = 3 + 17\mathrm{e}^{-t}$ and its Poisson's ratio is $\nu_0 = 0.38$. For the long fibers, these parameters are: $E_1 = 3 + 17\mathrm{e}^{-t/10}$ and $\nu_1 = 0.38$. Given the high volume fraction of inclusions (50%), the interpolative homogenization scheme is used. This composite was studied numerically by asymptotic homogenization in the Laplace domain (asymptotic homogenization method and 2D plane strain FE simulations are used as numerical method, square arrangement of the fibers is considered) in Yeong-Moo Yi *et al.* [109] and the time response is obtained by a Laplace numerical inversion method similar to the one used in this work (see appendix B.2). Predictions by mean-field homogenization schemes are available in Friebel *et al.* [33]. Our goal here is to reproduce homogenization results and check their accuracy against FE.

Prediction of the homogenized transverse plane strain tensile modulus is illustrated on figure 4.5. Plane strain tensile modulus (E_T^{PE}) is computed from a tensile test in a transverse direction with respect to the fibers so that the stress in the other transverse direction and deformation in the longitudinal

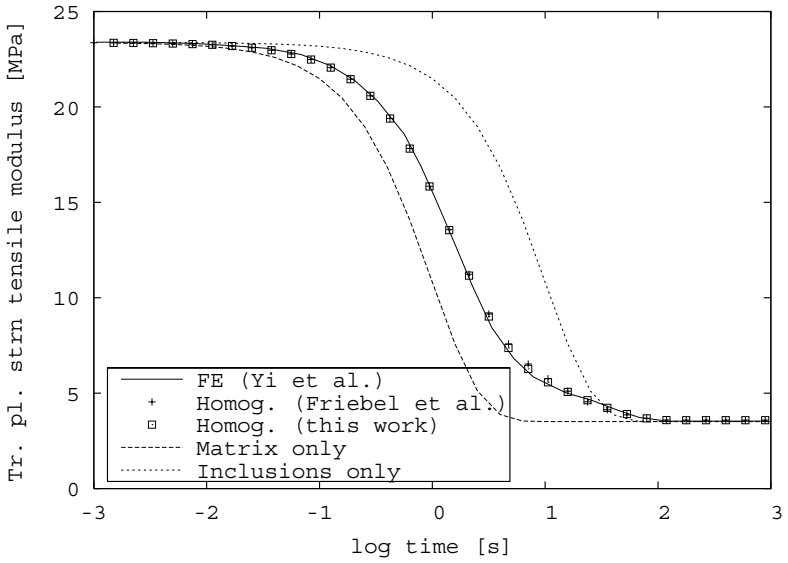

Figure 4.5: Prediction of the homogenized transverse plane strain tensile modulus of a two-phase linear viscoelastic composite.

direction are prevented. This can be computed from the components of the relaxation modulus in the Laplace-Carson domain as (direction 1 is aligned with the fibers):

$$E_T^{PE^*} = G^*_{3333} - \frac{G^*_{3322} G^*_{3322}}{G^*_{2222}}, \qquad \sigma^*_{33} = E_T^{PE^*} \varepsilon^*_{33}. \tag{4.65}$$

Our predictions are compared to the available results. Almost no difference can be seen between the two results obtained by mean-field homogenization (in both cases, 10 collocation points are used for the numerical Laplace inversion). Furthermore, a very good agreement is observed between homogenization and FE results.

Macroscopic response to a loading test can be computed with the help of equation (4.64). On figure 4.6, mean-field homogenization results for a uniaxial displacement test in the transverse direction to the fibers is illustrated. These results are confronted to 2D plane strain finite element simulations. For this, a quarter of unit cell corresponding to hexagonal array fibers arrangement is considered (see section 3.1). A very good agreement is observed for various strain rates. This means that the numerical inversion of the Laplace transform is done correctly as well as the computation of the convolution product. For a given loading path, evaluation of this convolution product is done incrementally

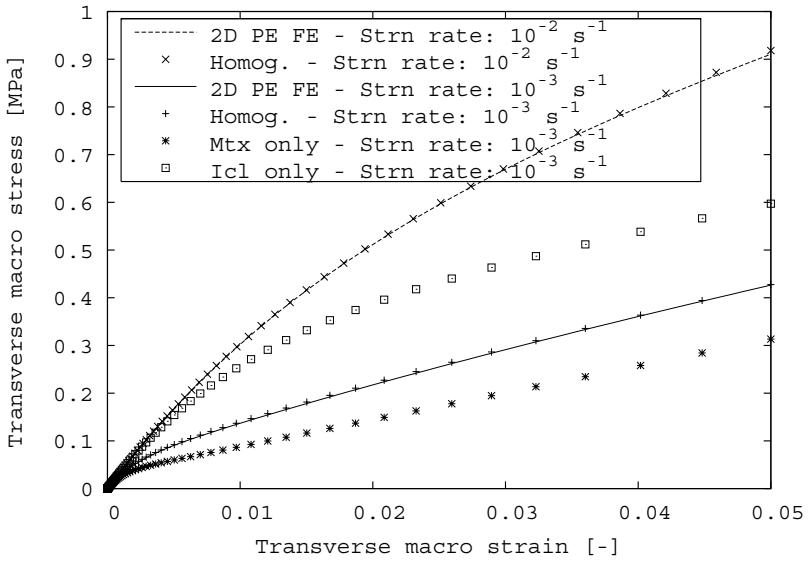

Figure 4.6: Prediction of the macroscopic response of a two-phase linear viscoelastic composite under uniaxial displacements.

in time from only the solution at the last time-step and given data over the increment, see appendix C for more details.

4.5 Conclusions

In this chapter, we focused on three subjects and presented their theory in detail. Firstly, major mean-field homogenization schemes for two-phase isothermal linear elastic composites are presented. Secondly, a general method allows to formulate the thermo-elastic version of any homogenization model defined by its isothermal strain concentration tensors. Thirdly, the problem of linear elastic composites is examined. All these homogenization schemes must be highly accurate since they are used as subproblems in the homogenization of nonlinear materials. For this reason, the predictions have been extensively validated against experimental data or FE results for numerous composite systems.

For thermo-elastic composites, we compared our predictions of the CTE with experimental data, either when each phase is isotropic or when the fibers present a transversely isotropic behavior. In both cases, the longitudinal and transverse values of the CTE were in excellent agreement with target results.

For linear viscoelastic composites, validations are done in both Laplace and

time domains. Predictions of a composite whose behavior is defined by Prony series are in excellent agreement with FE results. This guarantees the quality of the adopted homogenization scheme and of the numerical calculus (Laplace inversion, incremental evaluation of a convolution product).